Portable and Raman imaging usefulness to detect decaying on mortars from Punta Begoña Galleries (Getxo, North of Spain)

Cristina García-Florentino,[1] Maite Maguregui [2,*] Héctor Morillas, [1] Urko Balziskueta, [3] Agustin Azcarate, [3] Gorka Arana, [1] Juan Manuel Madariaga[1]

[1] Department of Analytical Chemistry, Faculty of Science and Technology, University of the Basque Country UPV/EHU, P.O. Box 644, 48080 Bilbao, Basque Country, Spain
[2] Department of Analytical Chemistry, Faculty of Pharmacy, University of the Basque Country UPV/EHU, P.O. Box 450, 01080 Vitoria-Gasteiz, Basque Country, Spain,
*e-mail: maite.maguregui@ehu.eus
[3] Department of Geography, Prehistory and Archaeology, University of the Basque Country UPV/EHU, P.O. Box 450, 01080 Vitoria-Gasteiz, Basque Country, Spain

ABSTRACT

Punta Begoña Galleries were built in 1918 in Getxo (Basque Country, North of Spain) but were abandoned in 1960. Nowadays their conservation state is very poor. In this work, portable Raman spectroscopy was applied to evaluate the original composition and possible deterioration products of the mortars used in the inner walls and those covering the concrete of the ceilings allowing us to select the most appropriate sampling points. In the laboratory Raman microscopy and Raman imaging, assisted with SEM-EDS, XRD and ED-XRF imaging, allowed to identify the key compounds to understand the deterioration processes taking place in the mortars of the Galleries. The main components of the mortars from the walls were calcite and gypsum. In some cases, alite (Ca_3SiO_5) and belite (Ca_2SiO_4) were identified; these components are characteristic of Portland cement clinker. The main components of the mortar covering the concrete were calcite, quartz, aragonite and gypsum. The aragonite identification confirmed the use of beach sand as the aggregate in the mortar. The concrete from the ceiling of the lower Gallery is covered with three different mortar layers; the outermost layer is covered with a black crust. In the three mortars the main components are similar to those used in the mortar covering the concrete from the upper Gallery. Thanks to Raman, ED-XRF and SEM-EDS imaging it was possible to map the distribution of the main components through the three mortar layers and also to identify the presence of dolomite ($[Ca(Mg(CO_3)_2]$) which was not possible to detect following single-point micro-Raman analyses.

Keywords: Portable Raman, Raman imaging, ED-XRF imaging, mortars, soluble salts

Introduction

Mortars are building materials formed by an aggregate (sand), water and a binder. This last component can be of different types, such as non-hydraulic lime, hydraulic lime or cement. Cement is a type of binder obtained by joint calcination of calcite and clay that later is milled producing the clinker, which is composed mostly by lime silicates (alite, $(CaO)_3SiO_2$ and belite, $(CaO)_2SiO_2$), lime aluminates (celite, $(CaO)_3Al_2O_3$) and lime ferritoaluminates (felite, $(CaO)_4(Al_2\ O_3)(Fe_2O_3)$).[1-2] These components react when water is added giving rise to other components that cause the hardening of the material. Sometimes gypsum is added as a setting agent, to finally obtain cement. When cement is mixed with rock aggregates like gravel and water, a mixture that sets and hardens giving rise to concrete is obtained.

Once mortars, cements and concretes are included in constructions and therefore exposed to the atmosphere, they can suffer from different degradation processes. Some of the most common degradation reactions are dissolution and leaching of the original components, reaction with the atmospheric pollutants leading to the formation of salts crystallized inside the pores (sub-efflorescences) or on the surface of the materials (efflorescences), formation of crusts [3] or more soluble compounds and hence more easily leachable, etc.[4] Some of the components of new formation can also lead to expansive reactions leading to the cracking of the material. As an example of this, the crystallization of secondary ettringite can be mentioned.[5] Soluble salt crystallization inside the porous system of the mortars also produces their deterioration. These salts are formed due to the ions included in the water used in the fabrication of the mortars and also due to those accessible to the material coming from underground or infiltration waters. Marine aerosols, as well as atmospheric pollutants (e.g. acid gases such as SO_x, NO_x, etc.), contribute to the formation of these salts in construction materials. Additionally, the metabolism of some living organisms can also be a source of some ions.[2]

In a porous system such as mortars, accumulated salts will crystallize and dissolved depending on the relative humidity of the environment. These successive crystallization/dissolution cycles are able to destroy the mortars mechanically because of the pressure generated during the crystallization process due to the growth of the crystals and to their hydration process. An example of this, is the thenardite (Na_2SO_4)/mirabilite ($Na_2SO_4{\cdot}10\ H_2O$) system.[6] In the case of the reinforced concrete, particular degradation reactions can take place due to the corrosion of the steel reinforcement. Portland cement provides an alkaline protection (pH=12-13) to the reinforcement of the concrete, in which the steel can remain without corrosion indefinitely. When cement content is reduced, the pH decreases to 10 leaving the steel without protection against water or humidity.[7] The alkaline protection provided by cement can be lost because different reasons. Some of them are the carbonation of

the concrete (reaction between the CO_2 present in the atmosphere and the $Ca(OH)_2$ of the cement) and depassivating ions (chlorides, sulfides or sulfates) action that break the electrochemical passivating layer existing between the steel and the concrete.[7] Chloride ions are especially present in marine environment, thus concretes exposed to a coastal atmosphere will suffer most likely this pathology.[7] Finally, construction materials can also suffer physical deterioration due to freeze-thaw cycles or thermal variations leading to material cracking or deteriorations due to biological activity.[2]

Until 1970- 1980 the characterization of historic mortars was mostly based on traditional wet chemical analysis.[8,9] However these methods are usually very laborious and the interpretation of the results is difficult and often impossible without a good previous knowledge of the nature of the different mortar components.[1,10] Nowadays, the majority of works related with mortar characterization, propose in a first step the optical microscopic analysis of the materials for qualitative identification and X-ray Diffraction (XRD) techniques to obtain a quantitative approximation of the mortar mineralogy. For further analysis, such as to identify the texture of the mineral aggregates, the shape of the crystals and their chemistry, Scanning Electron Microscopy equipped with an energy dispersive spectrometer analyzer (SEM-EDS) is usually employed.[5]

Raman spectroscopy can provide additional molecular information to the one provided by XRD due to its ability of identifying amorphous phases and minor compounds or traces present in specific areas of the material. In addition, portable Raman spectroscopy can provide the opportunity to obtained in situ molecular information of the mortars and also to identify degradation products that cannot be detected by XRD due to its minor presence.[6] Some Raman spectroscopic results can be corroborated by Ion Chromatography (IC) followed by a correlation analysis between cations and anions.[4]

In this work portable Raman spectroscopy was applied to evaluate the original composition and possible deterioration products of the mortars used in the inner walls of the Galleries and those covering the concrete of the ceilings from the Galleries. In the laboratory, Raman microscopy and Raman imaging analyses, assisted with SEM/EDS, XRD and Energy Dispersive X-ray Fluorescence (ED-XRF) imaging, were used with the aim to confirm the original compounds and its deteriorating products, aiming to understand the distribution of the main components of the mortars (in the walls and covering the concrete of the ceiling). Moreover, the soluble salt test was applied to the sampled mortars trying to confirm some Raman observations and to evaluate the concentration of the different new salts present on each mortar from the Galleries.

Experimental

Punta Begoña Galleries, sampling areas and samples description

Punta Begoña Galleries are located in Getxo, near the Ereaga beach, in the Basque Country (Spain). These Galleries were built in 1918 for an important businessman, Horacio Echevarrieta,[11] and nowadays they are abandoned and very deteriorated. The Galleries are composed of two levels: The upper Gallery and the lower Gallery. The upper Gallery is oriented to the Northwest and the lower Gallery is oriented to the Southwest. The ceiling of the upper Gallery is just below the gardens of Punta Begoña from which water can flow through, until entering inside the upper Gallery on rainy days. Some parts of the ceiling have been detached, showing the structure of the reinforced concrete covered with different mortar layers. The walls and the columns are composed by different decorative mortars whose different layers have been detached in some points. The lower Gallery is decorated in a similar way to the upper one.

The mortars/cements and concrete samples extracted from the Galleries were classified into samples of upper Gallery (named as UG) and lower Gallery mortars (named as LG) from the wall (e.g. MLG, mortar from lower Gallery) and reinforced concrete samples from the ceilings of upper Gallery and lower Gallery. The reinforced concrete samples from the ceiling of upper Gallery are covered with a single layer of a decorative mortar (sample named as MCUG, mortar over the concrete from upper Gallery). In all these sample types, a huge dissolution of the mortar/cement binder of the concrete gravel can be observed. However, in the case of the reinforced concretes from the ceiling of lower Gallery (sample called CLG, concrete from lower Gallery), the concrete is covered with three different mortar layers, L2, L3 and L4 from the most external one to the most internal one in contact with the concrete (see Fig. 1). In some parts on the top of L2 mortar layer, an additional very thin layer (L1) that can be a crust of new formation is observable.

Instrumentation and methodology

Portable Raman spectroscopy was used to perform an in situ screening of the mortars under study and in order to select the most suitable sampling areas. The sampling was performed in those areas where maximum spectral information was obtained and lower fluorescence effect was observed.

In the laboratory and to complete the in situ analyses, additional single-point Raman measurements were performed. Apart from that, Raman imaging was also performed

using a confocal Raman microscope to determine the distribution of the major compounds in the mortars. These results were compared with additional molecular analyses using X-ray Diffraction (XRD). To complete the mortars characterization, elemental analyses were also performed using Scanning Electron Microscopy coupled to an Energy Dispersive X-ray Spectrometer (SEM-EDS). In order to obtain the elements distribution on the whole stratigraphy of the mortars, Energy Dispersive X-ray Fluorescence (ED-XRF) imaging was also performed. Finally, to evaluate the salt content on the mortars, ion chromatography was employed.

Portable and laboratory Raman spectrometers

The in situ Raman measurements were performed using two portable Raman spectrometers (innoRam model, $B_{\&}WTEK_{INC.}$, Newark, EEUU). One of them is equipped with a 785 nm excitation wavelength (laser rated power > 300 mW) and the other one with a 532 nm excitation wavelength (laser rated power > 50 mW). The Raman measurements were performed directly placing the probe on the surface of the mortars under study. For the in situ measurements performed on the ceiling of the Galleries, a scaffolding mounted by the City Council of Getxo was used. The spectra were collected between 3000-65 cm^{-1} in the case of the instrument provided with 785 nm laser (4 cm^{-1} resolution spectra measured at 912 nm) and between 3750-65 cm^{-1} in the case of the instrument provided with 532 nm laser (5 cm^{-1} resolution spectra measured at 609 nm). Even though that these two lasers were used to obtain information, better results for this kind of materials were achieved with the 785 nm laser. The spectra were registered between 2-15 s and were accumulated between 5-20 times in order to improve the signal/noise ratio. Data acquisition was possible thanks to the $B_{\&}WSpec$ software ($B_{\&}WTEK_{INC.}$, Newark, EEUU).

In order to observe the distribution of the main components of all the mortar layers covering the concrete from the ceiling of the lower Gallery, Raman image analyses were performed using an InVia Raman microscope (Renishaw, Gloucestershire, UK). This spectrometer is coupled to a DMLM Leica microscope that can work with a huge range of objective lens (5x, 20x, 50x and 100x). It also has a Peltier cooled detector and 785 nm and 514 nm excitation wavelength lasers with rated powers of 350 mW and 50 mW respectively. The Raman image acquisition was performed using the StreamLine Plus configuration that is able to become the spherical spot of the laser in a line thanks to its special optical configuration. In this work the Raman image analyses were done using the 785 nm laser and the 20x objective lens. Once they were obtained the spectra from the selected area, a spectral treatment consisting on a base line correction and on a spectral filtration process was applied. In order to represent the Raman images, the interest regions/bands of the detected components were selected and one map per component was represented.

The spectral interpretation of the single-point Raman spectra obtained with the portable instruments was done using the Omnic V.7.2 (Nicolet) software while the obtained Raman images were treated with Wire 3.0 (Renishaw, UK) software. The Raman spectra interpretation was performed by comparison with spectra of pure standards registered in e-VISARCH and e-VISART [12] databases, as well as using Raman spectra contained in the on- line free access RRUFF database.[13]

X-ray Diffraction

XRD technique was also used to obtain a semiquantitative estimation of the major components (above 5%) present in the materials analyzed in situ by Raman spectroscopy. Before the analysis, each different mortar/cement layer was separated manually using a scalpel or a chisel and powdered in an agate mortar. XRD analyses were performed using a diffractometer (PANalytical Xpert PRO, Almelo, Netherlands) provided with a Cu tube ($\lambda\ Cu_{k\alpha average}$= 1,5418 Å, $\lambda\ Cu_{k\alpha 1}$= 1,5460 Å and $\lambda\ Cu_{k\alpha 2}$=1,54439 Å), a vertical goniometer (Bragg-Brentano geometry), programmable divergence slit, automatic sample exchanger, secondary graphite monochromator and PixCel detector. Additional information of the instrument and measurement conditions can be revised elsewhere.[14]

Energy Dispersive X-ray Fluorescence spectrometer (ED-XRF)

To compare the results obtained by Raman imaging regarding the mortar layers covering the concrete from the ceiling of the lower Gallery, elemental imaging analyses were also performed in the laboratory. With that purpose, elemental HyperMaps of the mortar layers over concrete were acquired in the millimeter scale using the M4 Tornado (Bruker Nano GmbH, Berlin, Germany) Energy Dispersive X-ray Fluorescence spectrometer. Analyses were performed under vacuum (20 mbar) in order to improve the detection of the lightest elements and the lateral resolution used for the spectral acquisitions was 1 mm. Details of the instrument can be checked elsewhere.[15] The Hyper Maps presented in this work were obtained using the M-Quant software package included in the M4 TORNADO software (Bruker Nano GmbH, Berlin, Germany) based on the application of Fundamental Parameters methods to obtain the quantitative results. Previous to obtain the Quantitative Hyper Maps, an elemental assignation and deconvolution of the spectral information was conducted. The Quantitative Maps were obtained according to the K-alpha line of each element showed in this work.

Scanning Electron Microscope coupled to an Energy Dispersive X-ray spectrometer (SEM-EDS)

To acquire additional elemental information of the mortar layers covering the concrete from the ceiling of the lower Gallery in a more microscopic scale, SEM-EDS was also used. Prior to the analysis, the samples were metalized with gold to improve their conductivity. The analyses were performed using an EVO 40 (Carl Zeiss, Germany) SEM and details of this instrument and the measurement conditions can be revised elsewhere.[16]

Ion Chromatography

To confirm the presence of some salts of new crystallization detected by Raman spectroscopy, the quantification of soluble salts (cations and anions) presented in mortar/cement and concrete samples was conducted using ion chromatography. In this case, it was also necessary to separate each of the layers to obtain individual information of the samples. With this aim, 0.5 g from each powdered layer were introduced in an oven at 60 ˚C for 24 h to dry them until constant weight. For the soluble salts extraction, 0.1 g of each sample were mixed with 100 ml of Milli-Q water and put in an ultrasonic bath for 2 hours. The aqueous extracts were filtered using a 0.45 µm nylon membrane filter and they were brought to a final volume of 100 ml. [17]

The soluble anion (F^-, Cl^-, NO_3^-, SO_4^{2-} and Br^-) and cation (Ca^{2+}, Li^+, NH_4^+ and Ba^{2+}) determination was performed with a Dionex ICS 2500-pressured ion chromatograph (Dionex Corporation, Sunnyvaley, California, EEUU) provided with an ion suppressor, a conductivity detector and an autosampler. Chromatographic peak integration and data acquisition was performed with Chromaleaon 6.60-SPIA software (Dionex Corporation, Sunnyvaley, California, USA).

With the data obtained from the ion chromatography, a correlation analysis between anions and cations was performed using The Unscrambler®7.6 (CAMO software, Oslo, Norway.[18] In this way, a high correlation value (above the critical value dependant of the confidence level and the freedom degrees) between an anion and a cation can be indicative of belonging to the same salt. The ionic concentrations were introduced in the software in (millimoles*ionic valence) per kilogram of dried sample in order to consider the charge effect of each dissolved ion when it is combined with the rest.

Results and discussion

In situ and laboratory molecular characterization of the mortars

With the aim of detecting the presence of major and minor components in the mortar samples Raman spectroscopy was used in an in situ way. In Table 1 a summary of all the identified components using the portable Raman spectrometers is presented. As can be observed in this table, the main components of the analyzed mortars are calcite ($CaCO_3$), quartz (SiO_2) and gypsum ($CaSO_4 \cdot 2H_2O$).

To obtain the semiquantitative composition of all the mortars, extracted mortar samples were analyzed using X-ray Diffraction (XRD). The obtained results are shown in Table 2. These values were calculated taking into account that the 100% of the sample composition is formed only by the components detected using XRD and thus, without considering minor or amorphous compounds that cannot be detected easily using this last technique.

As it can be observed in Table 2, all the samples contain calcite ($CaCO_3$) and quartz (SiO_2), and most of them gypsum ($CaSO_4 \cdot 2H_2O$). These results agree with the ones obtained by means of portable Raman spectroscopy. However, Raman analysis allowed also the identification of gypsum in MCUG that was not detected by XRD, probably because in this sample gypsum is present as minor compound (below 5%) and it is not widely distributed in all the mortar.

According to the XRD results, in some of the mortar samples, aragonite ($CaCO_3$), a calcite polymorph, was also a major component. This calcium carbonate polymorph was also detected by portable Raman spectroscopy (see Table 1) and its presence points out the use of beach sand as an aggregate in some cases, which was expected after the observation of some shell fragments in the walls of the Galleries. It is also important to remark the presence of halite (NaCl) in the mortar from the Lower Gallery (MLG) that could be deposited from the marine aerosol on the surface of the sample or crystallized inside the pores of the materials.

XRD analyses show that MLG and CLG-L2 are similar in composition. Probably both are lime mortars with low quartz content. This observation will be confirmed later using Raman imaging analyses. On the other hand, the mortar which covers the concrete from the upper Gallery (MCUG) is more similar to the L3 and L4 mortar layers covering the reinforced concrete from the Lower Gallery (CLG-L3 and L4).

The sample labeled as MLG (BC) is referred to the black layer that covers the mortar of the wall from the lower Gallery (MLG). As it can be seen in Table 2, the gypsum content is much higher than in the analysis performed on the mortar (MLG). The same

tendency is observed for the black layer (CLG-L1) over the most external mortar layer which covers the concrete from the lower Gallery (CLG-L2). These results suggest that both black layers can be related with the formation of black crusts.

In the Raman spectra acquired in situ on the mortar from the wall of the upper Gallery (MCUG), the repetitive presence (in more than 10 spectra) of lime silicates, alite [$(CaO)_3SiO_2$] and belite [$(CaO)_2SiO_2$)] were identified (see Fig. 2). Their presence can be related with the use of Portland cement as a binder of this mortar that remain un-reacted in the clinker hydration reaction.

Apart from the original components of the mortar, deterioration products such as nitrates were also identified in situ by Raman spectroscopy. The presence of nitratine ($NaNO_3$) in this mortar could be explained following two reactions. In the first one the NaCl present in the mortar could react with the atmospheric NO_x or nitrate ions present in the mortar and coming from infiltration waters to form the nitratine ($NaNO_3$). The second reaction that can explain the presence of nitratine in the mortar could take place in the atmosphere between the NaCl as particulate matter coming from the marine aerosol and the acid NO_x from the atmosphere. The nitratine formed as Secondary Marine Aerosol particles can be deposited latter in this mortar following a dry deposition process.[16]

In the mortar from the wall of the lower Gallery (MLG) calcite and gypsum were also detected by portable Raman spectroscopy as in the XRD analyses. In this mortar a band at 1025 cm^{-1} was also observable (see Fig. 3). This strong band can be related to the principal band of coquimbite or to its polymorph paracoquimbita ($Fe_2(SO_4)_3 \cdot 9H_2O$). However, it can also be related to the presence of γ-anhydrite (γ-$CaSO_4$).[19] The presence of this anhydrous calcium sulfate could be related with a dehydration process of the original gypsum present in the mortar which can crystallize in a different form to the most usual one, the β-anhydrite. According to some authors, the environmental temperature and the pressure, in this case the inner pressure of the material, can affect to the dehydration process of gypsum leading to the β or γ forms.[20] Around 1050- 1051 cm^{-1} the principal band of nitrates such as niter (KNO_3) and/or nitrocalcite ($Ca(NO_3)_2 \cdot 4H_2O$) was also detected. As in the obtained spectrum no secondary bands were observable, it cannot be distinguished between the presence of both nitrates. Therefore, as it will be explained later, soluble salts analysis of the mortars was conducted by means of ion chromatography in order to confirm the presence of nitrate salts and additional ones.

Below the same mortar from the wall of the lower Gallery, efflorescences (salts crystallized on the surface of the mortar) were visually observed (see Fig. 1 b). In the direct analyses performed on the efflorescences using the portable Raman spectrometers, thenardite (Na_2SO_4), gypsum and calcite were detected (see Fig. S 1a). Calcium carbonate is the main constituent of the mortars from the Gallery. Although

this carbonate is partially insoluble in water, it can be transformed at pH<9 into bicarbonate ($Ca(HCO_3)_2$), which is more soluble than the original carbonate. The formation of bicarbonate from the original carbonate can be promoted by the atmospheric CO_2. In the current modern atmosphere, the concentration of CO_2 is high. Therefore, carbonic acid (H_2CO_3) can be formed in the atmosphere reacting with the calcium carbonate from the mortar to form the soluble calcium bicarbonate (see reaction 1):

$$CaCO_3\,(s) + H_2O\,(l) + CO_2\,(g) \rightarrow Ca(HCO_3)_2 \quad \textbf{(1)}$$

The soluble calcium bicarbonate can be mobilized by rain-washing. But it can also precipitate into the surface of the material during the evaporation process, in the absence of rain, displacing the equilibrium of the reaction 1 to the left and promoting the crystallization of calcium carbonate, which can be deposited on the surface as an efflorescence. This reaction process is the most plausible that can take place in the mortar from the wall of the lower Gallery from Punta Begoña, but is not the only one. The ceilings of this lower Gallery are covered by gypsum, a partially soluble salt. Over the years, gypsum can be partially solubilised and the dissolved sulphate anions can migrate downwards to the walls. These sulphates, together with the calcium that can be present in solution in the material, can precipitate together in the surface of the walls as gypsum. That is why, using Raman spectroscopy this calcium sulphate salt was identified in the efflorescence of such walls.

In some punctual Raman spectra, apart from the mentioned compounds, natron ($Na_2CO_3{\cdot}10H_2O$) was also observed on the same efflorescences (see Fig. S 1b).

The concrete from Punta Begoña Galleries shows an important loss of the gravel binder. As it is too difficult to separate the binder from the gravel in the concrete, it was not possible to perform the XRD analysis of this binder. However, as Raman spectroscopy does not need to make a previous separation, this part of the concrete was directly measured using the portable Raman instruments. In the binder of the concrete gravel, hematite was more abundant than in the mortar layers, probably due to the reinforcement of the concrete. Additionally, bassanite ($CaSO_4{\cdot}0.5H_2O$) was identified. The presence of bassanite indicates that gypsum is suffering a dehydration process. The existence of a hydration/dehydration process of gypsum can lead to volume changes and therefore to cracks or fractures in the material, a pathology which is quite evident in the concrete of Punta Begoña Galleries.

In order to map the distribution of the main compounds of all the mortar layers covering the concrete from the lower Gallery (CLG) Raman imaging analysis was performed in one of the samples extracted from this area (see details of the sample in Fig. 1 and Raman images in Fig. 4). The layer 1 or black crusts formed on the external

mortar (L2) is not thick enough to obtain the molecular maps in the cross-section of the mortar layers over the concrete.

The Raman images of each compound showed in Fig. 4 are represented according to their respective main bands (calcite 1086 cm^{-1}, dolomite 1099 cm^{-1} and gypsum 1008 cm^{-1}) and according to 1162 cm^{-1} band for the case of silicates. The lateral or spatial resolution achieved in the Raman images showed in Fig. 4 was around 1.25 μm and the step width in x and y axes was 150 μm and 3.5 μm respectively.

According to the mapping results, calcite is distributed homogeneously and it is widely present in the mortar layers 2 and 3. In layer 4 a significant decrease of calcite presence and an increase in the presence of silicates can be observed. The non identification of silicates in layer 2 reaffirms the hypothesis that the aggregate used in this mortar layer was calcareous sand instead of silicate sand. In order to confirm this observation, a Raman imaging analysis of the layer 2 was performed. In the Fig. 4 right, the calcite distribution can be observed (image obtained at a 1.25 μm lateral resolution and (x, y) step width of (25 μm, 3.5 μm). In the microphotograph of this layer obtained under the optical microscope, fragments that can belong to the aggregate of the mortar can be observed (one of these fragments is marked with a circle in Fig. 4 right). According to the Raman imaging analysis, these fragments are made up of calcite, confirming again, the calcareous character of the aggregate in the mortar layer 2.

In mortar layers 2 and 3 the presence of dolomite [$CaMg(CO_3)_2$] was also identified, which was not found in the single-point Raman analysis. Regarding gypsum distribution, it is mainly present in layer 2, although it is also detected in layer 3 in a lesser extent. However, gypsum is not present in layer 4 confirming the results obtained with the XRD technique and the single-point Raman analysis.

Elemental imaging of the mortars at micro and millimeter scale

The Raman imaging analysis performed to describe the distribution of the principal compounds in the different mortar layers that form the CLG sample was complemented with an XRF imaging analysis of the same cross-section using a lateral resolution of 1 mm (mapped area around 25x20 mm^2).

In Fig. 5, the elemental distribution of the major elements present in the different mortar layers covering the reinforced concrete from the ceiling of the lower Gallery is shown. To construct the elemental images, the net counts of each element K_α lines were used. With this spectral information, quantitative maps were obtained thanks to the special software packed implemented in the instrument. Therefore, each pixel of the elemental distribution images presented in the Fig. 5 represents the concentration

of the corresponding element (black colour represents an absence of the element and the specific colour and its intensity represent a higher or lower concentration of the element in the mapped area). As it can be seen in Fig. 5, Ca is more or less distributed homogeneously through all the layers. However, S is concentrated in layer 2. This distribution matches with the distribution of gypsum obtained by Raman spectroscopy which is more abundant in the second layer and decreases towards the inner layers. The presence of S in this external part can also be related to the presence of a black crust (layer 1) characterized by SEM-EDS. Si and Fe are concentrated especially in layer 4 (see the delimitations of layer 4, the final part of the image does not correspond to layer 4 but with the concrete). The distribution of Si also confirms the silicate distribution observed by Raman spectroscopy in which silicates were concentrated in layer 4. Finally, Rb is more or less homogeneously distributed in all the layers.

The presence of Si in layer 4 was also confirmed by SEM-EDS, in which it was possible to see how in the parts that Ca was present, Si was not present and vice versa. In Fig. 6, SEM-EDS Ca and Si distribution maps are shown for mortar layer 4 in CLG sample. These distribution maps show clearly the presence of the calcareous binder (Ca distribution map) and of the aggregate (Si distribution map) from the mortar. In this layer, the nature of the aggregate is based on Si and not in Ca as in the case of layer 2. Due to the identification of an aggregate, this layer may be a mortar (binder and aggregate) discarding the possibility that could be a cement (a kind of binder).

Soluble salt quantification in the mortar samples

Considering the possibility that some of the mortar/cements could contain crystallized salts, a soluble salt test was also conducted with the aim to evaluate their nature and concentrations. The results obtained for the extraction of the soluble salts with Milli-Q water and their following analyses by ion chromatography are shown in Tables 3 and 4 respectively. The results of these samples are expressed with a confidence interval because the same sample was measured diluted and without diluting in order to adjust ion concentrations to the calibration.

According to the soluble salt test, all the analyzed mortars show the presence of chlorides, thus the influence of the marine aerosol (chloride salts deposition) is clearly confirmed with this additional analytical technique. With the XRD technique it was only possible to identify halite on the MLG sample, which is according to these quantitative results (see Table 3), the sample with the highest chloride content. The external mortar layers covering the concrete from lower Gallery (CLG) show the presence of fluorides that can also be present due to the influence of the marine aerosol.[21] In this same sample, nitrates were only detected in the inner layers and in a very low concentration. The higher nitrate content was detected in the black crust

over the mortar from the wall of the lower Gallery (MLG (BC)) and in the mortar itself (MLG). Considering that in this last mortar a high amount of sulphate efflorescences were detected (see Fig. S1) in situ by Raman spectroscopy, it was logical that in this mortar the concentration of sulphates determined by the soluble salt test was also the highest one. Moreover, this last mortar sample was the only one in which nitrocalcite and/or niter (a single band at 1050 cm^{-1}) presence was identified by single-point Raman analysis. Considering the low nitrate concentration in the rest of the samples, it was expected that Raman spectroscopy technique was not able to detect this kind of compounds.

Regarding the quantified cations using the soluble salt test, the concentration of sodium in the mortars from the walls of the lower Gallery is set around 5000 mg/kg. Some authors reported that the presence of 0.1% of Na_2O in the Portland cement could promote the formation of 0.45 kg of sodium carbonate in 100 kg of cement.[22] Taking into consideration the concentration of sodium in the mortar from the wall of the lower Gallery of Punta Begoña, the percentage in weight of Na_2O is set around 1.4 %. Therefore, it could be easy to justify the identification of natron ($Na_2CO_3 \cdot 10H_2O$) on the analyzed efflorescences formed after the dissolution process of the sodium compounds on the mortar itself. The presence of sodium compounds can leave free sodium cations in the material. These cations can react with the sulphates coming from the solubilisation of the gypsum from the material, giving rise to the formation of thenardite (Na_2SO_4). Thenardite can be present in equilibrium with the heptahydrated and/or decahydrated form of the sodium sulphate. This system can cause volume changes in the material, giving rise to the promotion of fissures and cracks.

With the obtained concentrations of cations and anions, coming from soluble salts, a correlation analysis between the anions and cations was performed. The correlation analysis for a 95% of confidence, six degrees of freedom and two-tailed analysis ($t_{critical}$ =2.45 and $r_{critical}$=0.84) indicates that Cl^--Na^+ and SO_4^{2-}-Ca^{2+} present a correlation that significantly differs from zero. These results are consistent with the ones obtained by Raman spectroscopy and XRD that show the existence of sodium chloride (NaCl) and gypsum ($CaSO_4 \cdot 2H_2O$) crystals. Although under the $r_{critical}$ value, Na^+ and NO_3^- also present a high correlation value as well as the one between Mg^{2+} and SO_4^{2-}. The high correlation value between Na^+ and NO_3^{3-} supports the hypothesis of the presence of nitratine ($NaNO_3$) on MUG sample as detected by Raman spectroscopy.

Conclusions

The results presented in this work evidence the necessity of combining Raman results with the ones extracted with additional techniques in order to contrast and complement the Raman evidences.[14] Sometimes, the Raman bands obtained are very weak, thus the assignations realized using these techniques can be uncertain. Powder XRD and ion chromatography after the use of the soluble salt test can be considered good alternative analytical techniques to confirm the mentioned Raman assignations.

Regarding the composition of the mortars (binder and aggregates) from Punta Begoña Galleries, it can be concluded that the composition of these binders and aggregates varied significantly among the analyzed mortars. The presence of alite and belite, components of the Portland cement initial clinker, in the mortar from the wall of the upper Gallery could suggest the use of cement as the binder of this specific mortar. Regarding the composition of the aggregates used in the mortars from the Galleries, it could be of calcareous or of siliceous nature. The mortars from the walls of the lower Gallery and the most external mortar layer covering the concrete from the lower Gallery belong to the first type of aggregate, while the mortar covering the concrete from the upper Gallery and the intermediate mortar and the mortar in contact with the concrete of the lower Gallery belong to the second type. In this last case, apart from quartz, aragonite was also detected, suggesting that beach sand was used as aggregate in this mortar. Finally, the binder (mortar) that joins the gravel of the concrete is similar to the mortars that cover the concrete from the upper Gallery.

The main pathologies identified in these mortars were two. The first one belongs to the dehydration/hydration process of gypsum from the mortar (anhydrite and bassanite presence). These cycles can cause stress in the material due to volume change, causing the formation of cracks, fissures, etc. Some of these physical problems are visually observable in the Punta Begoña Galleries.

The second pathology is related with the formation of efflorescences on and behind the mortars from the walls. In the areas where these salts are present, the mortar is partially detached. According to Raman results calcite ($CaCO_3$), gypsum ($CaSO_4 \cdot 2H_2O$), thenardite (Na_2SO_4) and sometimes natron ($Na_2CO_3 \cdot 10H_2O$) are the main constituents of these efflorescences. Apart from these salts, in the mortars from the lower and upper Galleries and using Raman spectroscopy, nitrate salts were also identified crystallized in the pores of the mortars. This observation was corroborated after the soluble salt test. The nitrate salts (in low concentration) in the mortars can be formed due to the reaction between nitrate anions transported in the infiltration waters and the corresponding solubilised cations from the mortar itself. The atmospheric NO_x can be also an additional nitrate source (wet deposition of the NO_x) to explain the formation of nitrates in the mortars from Punta Begoña Galleries.

Acknowledgements

This work has been funded by the Ministry of Economy and Competitiveness (MINECO) and the European Regional Development Fund (FEDER) through the project DISILICA-1930 (ref. BIA2014-59124-P) and by the cooperation agreement between the University of the Basque Country (UPV/EHU) and the City Council of Getxo (OTRI2014-0639). C. García-Florentino is grateful to the University of the Basque Country (UPV/EHU) who funded her pre-doctoral fellowship. Technical support provided by Raman-LASPEA Laboratory and General X-ray Service of the SGIKer (UPV/EHU, MICINN, GV/EJ, ERDF and ESF) is also gratefully acknowledged.

References

[1] J. Elsen, Cem. Concr. Res. **2006**; *36*, 1416.
[2] S.K. Duggal, Building Materials, New Age Intern. Publ., New Delhi, **2008**.
[3] C. Sabbioni, Sci. Total Environ. **1995**; *167*, 49.
[4] M. Maguregui, A. Sarmiento, I. Martinez-Arkarazo, M. Angulo, K. Castro, G. Arana, N. Etxebarria, J.M. Madariaga, Anal. Bioanal. Chem. **2008**; *391*, 1361.
[5] H. Morillas, I. Marcaida, M. Maguregui, J.A. Carrero, J. M. Madariaga, Sci. Tot Environ. **2016**; *542*, 716.
[6] M. Maguregui, U. Knuutinen, I. Martinez-Arkarazo, A. Giakoumaki, K. Castro, J.M. Madariaga, J. Raman Spectrosc. **2012**; *43*, 1747.
[7] J.P. Broomfield, Corrosion of Steel in Concrete: Understanding, investigation and Repair, CRC Press, Boca Raton, **2006**.
[8] H. Jedrzejewska, Stud. Conserv. **1960**; *5*, 132.
[9] E.B. Cliver, Bull. Assoc. Preserv. Technol. **1974**; *6*, 68.
[10] Mortars, cements and grouts used in the conservation of historic building, Proceedings of the ICCROM symposium, Rome, **1981**; 297.
[11] B. Estornés Lasa, in *Horacio Echevarrieta Maruri*, *Auñamendi Eusko Entziklopedia*, Euskomedia fundazioa, Donosti, **2008**.
[12] K. Castro, M. Pérez-Alonso, M. D. Rodríguez-Laso, L. A. Fernández, and J. M. and Madariaga, *Anal. Bioanal. Chem.* **2005**; *382*, 248.
[13] R.T. Downs. "The RRUFF Project: an integrated study of the chemistry, crystallography, Raman and infrared spectroscopy of minerals". Program and Abstracts of the 19th General Meeting of the International Mineralogical Association in Kobe, Japan. O03-13, **2006**.
[14] H. Morillas, M. Maguregui, C. Paris, L. Bellot-Gurlet, P. Colomban, J.M. Madariaga, Microchem. J. **2015**; *123*, 148.
[15] H. Morillas, M. Maguregui, C. García-Florentino, J.A. Carrero, I. Salcedo, J.M. Madariaga, Environ. Res. **2016**; *147*, 218.
[16] H. Morillas, M. Maguregui, C. García-Florentino, I. Marcaida, J.M. Madariaga, Sci. Tot. Environ. **2016**; *550*, 285.

[17] N. Prieto-Taboada, O. Gómez-Laserna, I. Martinez-Arkarazo, M. A. Olazabal, and J. M. Madariaga, *Ultrason. Sonochem.* **2012**; *19*, 1260.
[18] *The Unscrambler® 7.6*. Trodheim, Norway: Camo Asa, **2005**.
[19] N. Prieto-Taboada, O. Gómez-Laserna, I. Martinez-Arkarazo, M.A. Olazabal, J.M. Madariaga, Anal. Chem. **2014**; *86*, 10131.
[20] P. Comodi, A. Kurnosov, S. Nazzareni, L. Dubrobinsky, *Phys. Chem. Miner.* **2012**; *39*, 65.
[21] A. Lewandowska, L. Falkowska, and J. Jóźwik, *Environ. Sci. Pollut. Res. Int.* **2013**; *20*, 6109.
[22] M. Steiger, S. Asmussen, *Geochim Cosmochim. Acta.* **2008**; *71*, 4291.

Tables

Table 1. Compounds identified in the mortars and concretes under study using the two portable Raman spectrometers.

Samples	Original components	Transformation/Deterioration Products
MUG	**Calcite** (main bat at 1085 cm^{-1}) **Gypsum** (main band at 1008 cm^{-1}) **Alite** (main band at 838 cm^{-1}) **Belite** (main band at 861 cm^{-1})	**Nitratine** (main band at 1067 cm^{-1})
MLG	**Calcite** (main band at 1086 cm^{-1}) **Gypsum** (main band at 1007 cm^{-1}) **Hematite** (main band at 292 cm^{-1})	**γ-Anhydrite** (main band at 1025 cm^{-1}) **Nitrocalcite/niter** (main band at 1050-1051 cm^{-1})
MCUG	**Calcite** (main band at 1085 cm^{-1}) **Gypsum** (main band at 1008 cm^{-1}) **Quartz** (main band at 467 cm^{-1}) **Aragonite** (main band at 1084 cm^{-1})	
CLG	**Calcite** (main band at 1085 cm^{-1}) **Gypsum** (main band at 1008 cm^{-1}) **Quartz** (main band at 467 cm^{-1}) **Aragonite** (main band at 1086 cm^{-1}) **Hematite** (main band at 292 cm^{-1})	**Bassanite** (main band at 1015 cm^{-1})

Table 2. XRD semiquantitative estimation for the major components identified in the mortar samples.

Sample	Calcite %	Quartz %	Gypsum %	Aragonite %	Halite %
MLG	88	1	10	-	1
MLG (BC)	64	3	33	-	-
MCUG	36	59	-	5	-
CLG-L1	74	2	24	-	-
CLG-L2	89	1	10	-	-
CLG-L3	38	53	3	6	-
CLG-L4	36	49	-	15	-

Table 3. Soluble anion concentrations (mg/kg) in the mortar samples from Punta Begoña Galleries.

Anion	Concentration (mg/kg dried sample)						
	MCUG	CLG-L1	CLG-L2	CLG-L3	CLG-L4	MLG(C)	MLG(BC)
F^-	<LOQ	1890 ± 170	904 ± 21	643 ± 68	<LOQ	<LOQ	<LOD
Cl^-	3964 ± 174	1438 ± 39	678 ± 11	1589 ± 47	1311 ± 12	5650 ± 270	4690 ± 470
NO_3^-	339 ± 28	N.D	<LOQ	482 ± 97	257 ± 36	570 ± 72	1078*
SO_4^{2-}	6420 ± 110	$(1.89 \pm 0.25)\cdot10^5$	$(5.54 \pm 0.11)\cdot10^4$	15470 ± 210	8320 ± 160	$(8.61 \pm 0.49)\cdot10^4$	$2.45\ 10^5$*
Br^-	N.D	N.D	N.D	N.D	N.D	N.D	N.D

*→ Single value due to lack of mass

<LOQ → Concentration under the limit of quantification but above the limit of detection

<LOD → Concentration under the limit of detection

N.D → No signal on the chromatogram, non-detected analyte

Table 4. Soluble cations concentrations (mg/kg) in the mortar samples from Punta Begoña Galleries.

Cation	Concentration (mg/kg dried sample)						
	MCUG	CLG-L1	CLG-L2	CLG-L3	CLG-L4	MLG	MLG(BC)
Na^+	3969 ± 81	1137 ± 61	357 ± 20	923 ± 58	<LOQ	4800 ± 600	3350 ± 420
K^+	963 ± 20	188 ± 36	<LOQ	737 ± 84	482 ± 12	<LOQ	<LOQ
Mg^{2+}	<LOQ	546 ± 25	<LOQ	<LOQ	<LOQ	426 ± 23	<LOQ
Ca^{2+}	$(1.39 \pm 0.19)\cdot10^4$	$(8.90 \pm 0.58)\cdot10^4$	32650 ± 850	19210 ± 650	12970 ± 650	$(4.10 \pm 0.19)\cdot10^4$	$(1.078 \pm 0.086)\cdot10^5$
Li^+	<LOD	N.D	N.D	N.D	N.D	N.D	N.D
NH_4^+	<LOD	N.D	N.D	N.D	N.D	N.D	N.D
Ba^{2+}	N.D	N.D	N.D	N.D	N.D	N.D	N.D

<LOQ → Concentration under the limit of quantification but above the limit of detection

<LOD → Concentration under the limit of detection

N.D → No signal on the chromatogram, non-detected analyte

Figure captions

Fig. 1. A general view of Punta Begoña lower Gallery showing (a) a fragment of the concrete detached from the ceiling with the three mortar layers (L2, L3 and L4) covering it and the black crust (L1) formed on the surface of the mortar layer L2 (b) detached external mortar from the wall and the efflorescences formed on it.

Fig. 2. Raman spectrum acquired in situ with the 785 nm laser on the mortar from the upper Gallery showing the presence of gypsum, calcite, alite and belite (see also Raman spectra of gypsum and calcite standards).

Fig. 3. Raman spectra acquired in situ with the 785 nm laser on the binder from the concrete showing the bands of bassanite (B), and on mortar from the wall of the lower Gallery showing bands of calcite (C) and gypsum (G) together with the bands at 1025 cm^{-1}.

Fig. 4. Molecular distribution of the main compounds on the cross-section of sample CLG including all the mortar layers (L2, L3 and L4) over the concrete (on the left) and the calcite distribution inside the Layer 2 (on the right).

Fig. 5. Visible image of the mortars on the concrete (top left) and elemental maps of the main elements detected on the mentioned mortars from Punta Begoña lower Gallery ceiling.

Fig. 6. Ca distribution map (left) and Si distribution map (right) in mortar layer 4 in CLG sample.

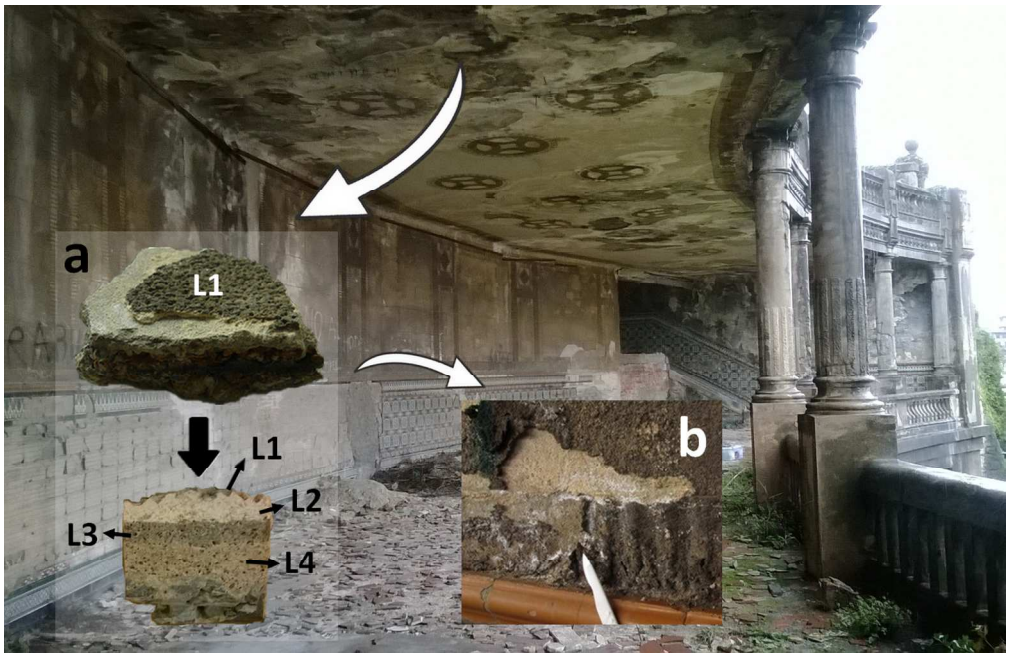

Figure 1. A general view of Punta Begoña lower Gallery showing (a) a fragment of the concrete detached from the ceiling with the three mortar layers (L2, L3 and L4) covering it and the black crust (L1) formed on the surface of the mortar layer L2 (b) detached external mortar from the wall and the efflorescences formed on it.
500x323mm (72 x 72 DPI)

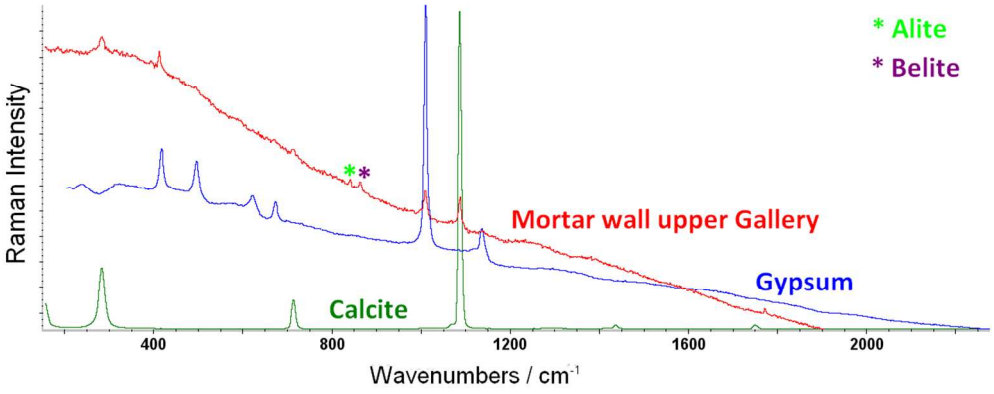

Figure 2. Raman spectrum acquired in situ with the 785 nm laser on the mortar from the upper Gallery showing the presence of gypsum, calcite, alite and belite (see also Raman spectra of gypsum and calcite standards).
456x185mm (72 x 72 DPI)

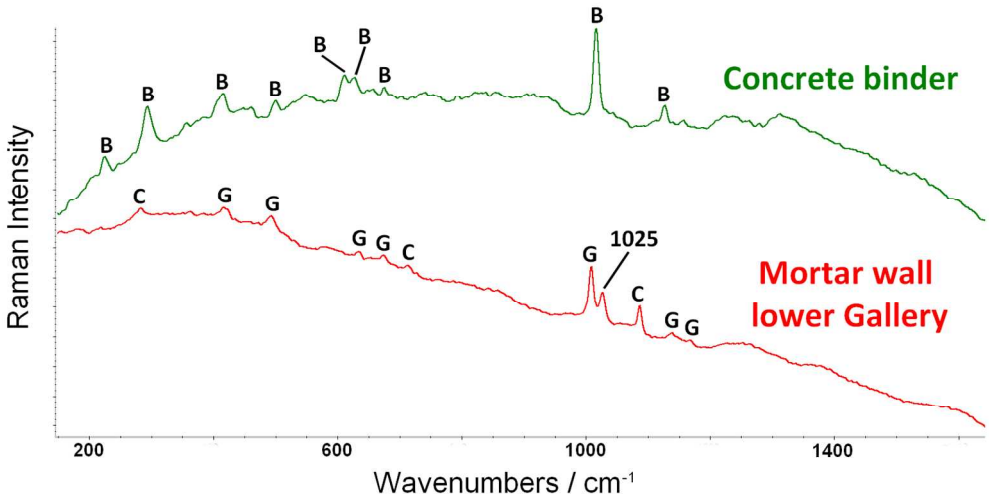

Figure 3. Raman spectra acquired in situ with the 785 nm laser on the binder from the concrete showing the bands of bassanite (B), and on mortar from the wall of the lower Gallery showing bands of calcite (C) and gypsum (G) together with the bands at 1025 cm-1.
208x107mm (200 x 200 DPI)

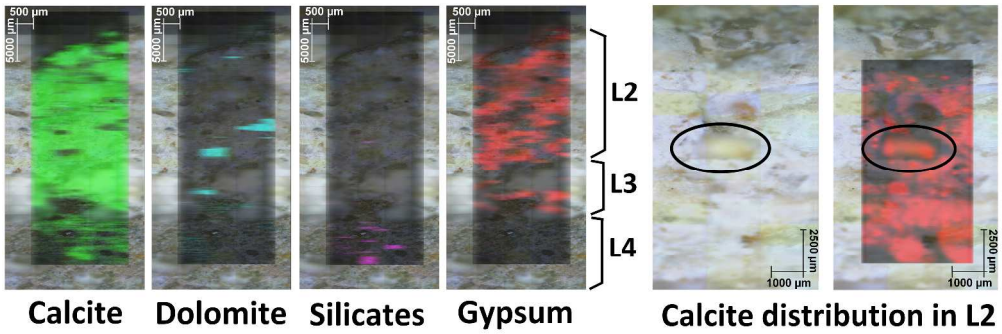

Figure 4. Molecular distribution of the main compounds on the cross-section of sample CLG including all the mortar layers (L2, L3 and L4) over the concrete (on the left) and the calcite distribution inside the Layer 2 (on the right).
1750x599mm (120 x 120 DPI)

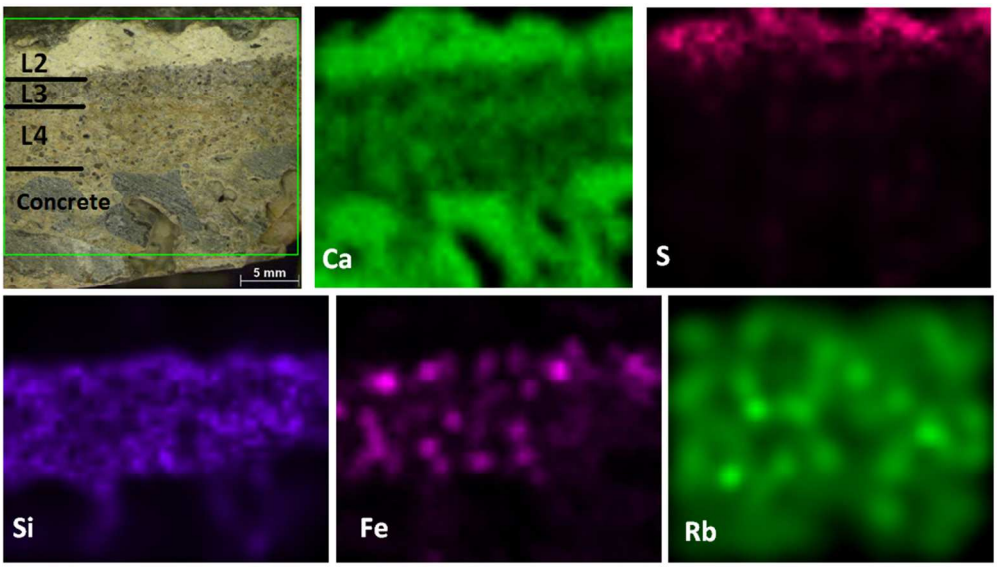

Figure 5. Visible image of the mortars on the concrete (top left) and elemental maps of the main elements detected on the mentioned mortars from Punta Begoña lower Gallery ceiling.
283x160mm (96 x 96 DPI)

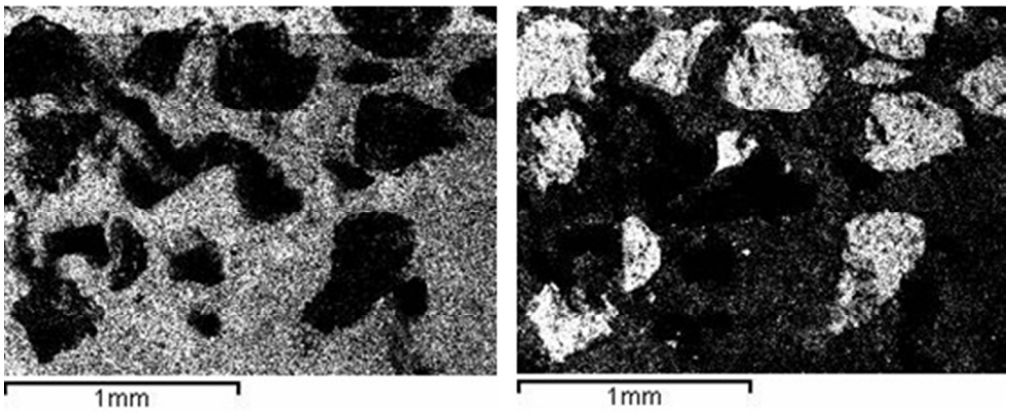

Figure 6. Ca distribution map (left) and Si distribution map (right) in mortar layer 4 in CLG sample.
145x60mm (96 x 96 DPI)